J. Fluid Mech. (1987), *vol.* 183, *pp.* 451–465
Printed in Great Britain

Subharmonic resonance of nonlinear cross-waves

By SETH LICHTER AND JERRY CHEN

Aerospace and Mechanical Engineering Department, University of Arizona, Tucson, AZ 85721, USA

(Received 30 July 1986 and in revised form 3 April 1987)

The evolution equation governing wavemaker-generated cross-waves near a cutoff frequency in an infinitely deep, infinitely long channel is shown to be the nonlinear Schrödinger equation with a homogeneous boundary condition at the wavemaker. With the inclusion of an empirically determined damping coefficient, numerical results for growth rate, slow modulation period, and wave amplitude show good agreement with previous experiments. The results also describe observations of trapped and propagating solutions.

1. Introduction

Cross-waves have been studied for over one hundred years, and Garrett's (1970) paper contains a review of the early literature. However, it is still baffling to see a wave tank in which cross-waves appear at one-half the forcing frequency, with their crests at right angles to the wavemaker. This puzzling observation, in fact, hints at the difficulty in reconciling, mathematically, the wavemaker boundary condition with the cross-wave field. Many experimental results (Barnard & Pritchard 1972) still have scant theoretical support, and recent observations of trapped and chaotic solutions in closely allied phenomena (Wu, Keolian & Rudnick 1984; Ciliberto & Gollub 1985) further stimulate interest in the nonlinear character of cross-waves.

Cross-waves are generated in a channel by a symmetric wavemaker (i.e. one for which the wavemaker displacement is constant across the channel at any given depth). A similar instability is Faraday resonance in a trough (Miles 1984; Wu *et al.* 1984). In both phenomena, there is a nonlinear parametric resonance in the neighbourhood of the cutoff frequencies (i.e. the natural frequencies based on channel width).

Barnard, Mahony & Pritchard (1977) and Jones (1984) update Garrett's review. Barnard *et al.* investigated steady-state waves generated by a (antisymmetric) plane paddle oscillating about a vertical shaft. In this case, the waves are forced directly at the fundamental frequency. Aranha, Yue & Mei (1982) made a numerical study of the nonlinear Schrödinger equation describing time-dependent inviscid acoustic modes in a duct. The response is once again forced directly, as is evident by the inhomogeneous wavemaker boundary condition (cf. Aranha *et al.*, equation 2.31*b*).

For a symmetric wavemaker in a channel, Jones found an implicit boundary condition, implying that, as an initial-value problem, the parametrically excited cross-waves will develop from the forced quiescent state only if initially perturbed. He found good agreement between his linearized equations and measurements by Barnard & Pritchard (1972) near the stability margin. Miles (1985) found a hyperbolic secant solution which describes a trapped soliton solution to Jones's equations.

This paper is concerned with the slow modulation (in both space and time) of

parametrically excited cross-waves in a channel in the presence of damping. We differ from Jones (1984) and the earlier work of Mahony (1972) in that our interest is cross-waves near saturation for which the cross-wave amplitude is considerably larger than the wavemaker amplitude. At these large amplitudes, it was found necessary to rescale the equations derived by Jones with a factor which depends on wavemaker shape. The governing equation for the complex amplitude A is the cubic nonlinear Schrödinger equation

$$iA_\tau + A_{XX} + \Lambda A + |A|^2 A = 0,$$

with the wavemaker boundary condition

$$A_X = iA^* \quad \text{at } X = 0,$$

where Λ is the detuning parameter.

For quantitative comparison with data, it is necessary to augment the inviscid equation with an empirically derived damping coefficient. Numerical results are presented which are in good agreement with the growth rate, slow modulation period, spatial structure, and amplitude measurements of Barnard & Pritchard. The numerical results also reveal propagating modes, first observed experimentally by Barnard & Pritchard, and trapped solutions. The inviscid trapped solution found by Miles (1985) is shown to fall outside the region of linear instability. The numerical viscous trapped solutions, however, do occur inside the linear instability region.

2. Formulation

Variables are non-dimensionalized through the use of length l and time $(l/g)^{\frac{1}{2}}$, where g is the gravitational acceleration. The channel is considered infinitely deep with the origin at the undisturbed free surface and z positive upwards. Rigid walls are at $y = 0$ and $n\pi/\alpha$, where $\alpha = n\pi l/b$, b is the dimensional width, and n, the transverse mode number, is easily visualized as equal to twice the number of wavelengths spanning the y-direction. The mean location of the wavemaker is at $x = 0$, and the channel extends to $x \to \infty$.

The velocity field $\bar{u} = \nabla\Phi$ is assumed inviscid, incompressible and irrotational, where $\Phi(x, y, z, t)$ is the velocity potential. The governing equation is

$$\nabla^2\Phi = 0. \tag{1}$$

The free-surface boundary conditions are

$$\Phi_z = \zeta_t + \Phi_x\zeta_x + \Phi_y\zeta_y \quad \text{on } z = \zeta(x, y, t), \tag{2}$$

$$\Phi_t + \zeta + \tfrac{1}{2}(\Phi_x^2 + \Phi_y^2 + \Phi_z^2) = 0 \quad \text{on } z = \zeta(x, y, t), \tag{3}$$

where surface tension is neglected. The normal velocity vanishes at the sidewalls:

$$\Phi_y = 0 \quad \text{on } y = 0, \frac{n\pi}{\alpha} \tag{4}$$

and the velocity potential vanishes at great depth:

$$\Phi = 0 \quad \text{on } z \to -\infty. \tag{5}$$

The wavemaker oscillates with frequency ω and amplitude $\epsilon \ll 1$ about $x = 0$ according to

$$x = \epsilon F(z) \sin \omega t.$$

For a plane flap hinged at $z = -d$,

$$F(z) = \begin{cases} 1+\dfrac{z}{d} & -d < z \leqslant 0, \\ 0 & z \leqslant -d. \end{cases}$$

On the wavemaker, the kinematic boundary condition is

$$\Phi_x = \epsilon\left(\frac{\partial}{\partial t} + \Phi_z \frac{\partial}{\partial z}\right)[F(z)\sin\omega t] \quad \text{on } x = \epsilon F(z)\sin\omega t. \tag{6}$$

Equations (1)–(6), together with a radiation boundary condition as $x \to \infty$, constitute the problem statement.

The multiple-scale perturbation method is used to look for a weakly nonlinear solution for which the complex amplitude A of the cross-wave velocity potential is a function of a large spatial scale X and a slow time τ,

$$\psi = \epsilon\alpha^{-\frac{3}{2}}[A(X,\tau)\,\mathrm{e}^{-\mathrm{i}\gamma t} + *]\,\mathrm{e}^{\alpha z}\cos\alpha y,$$

where the subharmonic cutoff frequency $\gamma = \alpha^{\frac{1}{2}}$, and * denotes the complex conjugate. Using the scalings

$$X = \epsilon\alpha x, \quad \tau = \epsilon^2\gamma t, \tag{7a,b}$$

one can follow Jones's (1984) analysis to obtain the slow modulation equation (see also Miles 1985)

$$\mathrm{i}A_\tau + \tfrac{1}{4}A_{XX} + \Lambda A + \tfrac{1}{2}|A|^2 A = 0, \tag{8a}$$

$$A_X = \mathrm{i}RA^* \quad \text{at } X = 0, \tag{8b}$$

where

$$\Lambda = \frac{\omega/2\gamma - 1}{\epsilon^2} - 0.202G^2, \tag{9a}$$

$$G = 4\alpha^2 \int_{-\infty}^{0} F(s)\,\mathrm{e}^{4\alpha s}\,\mathrm{d}s, \tag{9b}$$

$$R = \alpha\left[\int_{-\infty}^{0} \mathrm{e}^{2\alpha s}\frac{\mathrm{d}F}{\mathrm{d}s}\mathrm{d}s - 2F(0) + 4\alpha\int_{-\infty}^{0} F\,\mathrm{d}s\right]. \tag{9c}$$

The definition of Λ in (9a) is slightly different from Jones (1984) because of straining the t-coordinate instead of the y-coordinate. While Jones's original scaling is well suited to his analysis of the initial growth of cross-waves, from Barnard & Pritchard's (1972) experimental results for $n = 2$ and from Lichter & Shemer (1986), we find $R = O(\epsilon^{-\frac{1}{2}})$. For these cases then, the original scaling leads to $|A|$ being greater than $O(1)$; this indicates the need to rescale the equations. We set

$$\hat{X} = RX, \quad \hat{\tau} = \tfrac{1}{4}R^2\tau,$$

$$\hat{A} = \frac{\sqrt{2}}{R}A, \quad \hat{\Lambda} = \left(\frac{2}{R}\right)^2\Lambda.$$

Omitting the circumflex, (8) can now be written as

$$\mathrm{i}A_\tau + A_{XX} + \Lambda A + |A|^2 A = 0, \tag{10a}$$

$$A_X = \mathrm{i}A^* \quad \text{at } X = 0. \tag{10b}$$

The introduction of R as a rescaling parameter implies that the ultimate scaling is formulated upon ϵR. This composite scaling parameter is independent of the lengthscale l. The necessity to rescale can be understood heuristically as follows.

The amplitude of the harmonic progressing wave is proportional to an integral of the wavemaker shape times a decaying exponential in depth, see Havelock (1929) or Jones's (1984) equation (3*c*); so only that portion of the wavemaker near the surface is relevant to progressing-wave growth. However, the cross-wave amplitude, through R, depends on a term that is an integral of the wavemaker shape $F(z)$; a wavemaker of considerable depth, then, can result in large-amplitude cross-waves and small progressing waves, see also Garrett (1970).

3. Viscous damping

As noted by Barnard *et al.* (1977) in the case of antisymmetric forcing, the inviscid formulation must be augmented by a damping term before quantitative comparison with measurements (see also Miles 1984). Barnard *et al.* derived an expression for the damping at the walls of the channel and then evaluated the coefficients empirically. Applying their matched asymptotic expansion procedure to the present case yields the result, identical with theirs, that the real coefficient Λ in the inviscid equation (10*a*) is replaced by

$$\Lambda \rightarrow \lambda + \mathrm{i}L,$$

where λ is the observed frequency detuning and L is an empirical damping coefficient. The empirical λ will then incorporate the viscous correction as well as the interaction G from the progressing wave, though this last contribution is small (Jones 1984). The coefficient L can be determined from Barnard & Pritchard's (1972) measurements of the linear growth rate at the stability margin. Using the solution to the linearized equation (10) and Barnard & Pritchard's figure 2 (*a*), we find $0.0114 \leqslant (\epsilon R)^2 L \leqslant 0.0312$ for wavemaker amplitudes $0.0065 \leqslant \theta \leqslant 0.0128$. From linear analysis (Barnard *et al.* 1977; Miles 1984), $(\epsilon R)^2 L$ is expected to be constant for all cases at $n = 2$. So, for comparison with the experiments, we chose $(\epsilon R)^2 L = 0.0154$.

Augmented by the damping term, all solutions are damped for sufficiently large X, and we can finally write the boundary condition at infinity as

$$A = 0 \quad \text{on } X \rightarrow \infty. \tag{11}$$

4. Numerical approach

Equation (10) is solved numerically by a semi-implicit (Crank–Nicolson) finite-difference scheme similar to the one used by Aranha *et al.* (1982):

$$A_{m+1} = A_m - \tfrac{1}{2}\mathrm{i}\Delta\tau\left[\frac{1}{\Delta X^2}\delta_{XX}(A_{m+1}+A_m) + (\lambda+\mathrm{i}L)(A_{m+1}+A_m) + (|\tilde{A}_{m+1}|^2 A_{m+1} + |A_m|^2 A_m)\right], \tag{12a}$$

where $A_m = A(X, m\Delta\tau)$, δ_{XX} is the second-order central-difference operator in the X-direction, and

$$\tilde{A}_{m+1} = A_m - \mathrm{i}\Delta\tau\left[\frac{1}{\Delta X^2}\delta_{XX} A_m + (\lambda+\mathrm{i}L) A_m + |A_m|^2 A_m\right]. \tag{12b}$$

A sufficiently large domain for X was used to ensure that, for the times presented, the outer boundary effects were negligible. Due to the complex-conjugate term appearing in the boundary condition, a tridiagonal solver cannot be used here. However, dividing A into real and imaginary parts, the discretized system of (12)

associated with the boundary conditions is still a banded matrix. As the waves are driven by an implicit homogeneous boundary condition, a non-zero initial condition is necessary to excite the cross-waves. To satisfy the boundary conditions at $X = 0$ and $X \to \infty$, the initial condition for the scheme is chosen as

$$A(X, 0) = a_0(1 - \mathrm{i})\,\mathrm{e}^{-X}, \tag{13}$$

where a_0 is a real constant for which we chose $a_0 = 0.01$ for all cases presented. In earlier runs, using a_0 as small as 0.0001 gives no discernible difference compared with $a_0 = 0.01$.

Equation (12) is consistent, and the truncation error of the scheme is second order in time and space. It is easy to prove that iterations on the nonlinear term in (12*a*) are not necessary to improve the accuracy of the scheme. Equation (12) was stable for all of our runs.

The determination of computational step sizes was based on experience with the code testing and the variation of numerical results for different $\Delta\tau$ and ΔX. All of the viscous calculations were done with $\Delta\tau = 0.025$ and $\Delta X = 0.05$. For the inviscid case, which was more sensitive, $\Delta\tau = 0.01$ for $\tau \leqslant 5$, $\Delta\tau = 0.0025$ for $\tau > 5$, and $\Delta X = 0.05$.

For $L > 0$, a solution to the linearized equation (10) was used for the code testing. For the nonlinear equation with $L = 0$, the scheme was tested against a known solitary-wave solution of (10*a*) with an implicit homogeneous boundary condition at $X = 0$.

5. Results

5.1. *Inviscid results*

As noted in §3, viscous effects must be taken into account to allow quantitative comparison with measurements. However, the qualitative features of the experimental results are already present in the inviscid results. From figure 1, linear growth followed by a nonlinear rise to finite amplitude is evident. In general, the final state appears not to be of constant amplitude. As can be seen from the space–time evolution in figure 2, variations in amplitude are accompanied by disturbances which propagate away from the wavemaker.

5.2. *Viscous results*

To show the scope and limitations of the analysis, our numerical calculations are compared with Barnard & Pritchard's (1972) experiments for mode $n = 2$, for which the observed cutoff frequency was $\pi/0.22202\ \mathrm{s}^{-1}$. These experiments were carried out in a rectangular channel, 30.6 cm wide and 270 cm long, with water 16.4 cm deep. The wavemaker was a plane flap, hinged at the base, at one end of the wavetank. An absorbing beach was at the opposing end of the tank.

For these experiments, to recover dimensional quantities, slow time τ is multiplied by $(b/n\pi g)^{\frac{1}{2}}(2/\epsilon R)^2$ and X by $b/(n\pi\epsilon R)$. To facilitate comparison with the experimental results, we adopt Barnard & Pritchard's (1972) notation for the wavemaker angular displacement θ. Also, as noted in §3, linear analysis implies that $\theta^2 L$ is constant. So, for Barnard & Pritchard's forcing frequency, $\omega = 2\pi/0.22198\ \mathrm{s}^{-1}$, ϵR can be replaced by 16.455θ, $\theta^2 L = 5.695 \times 10^{-5}$, and $\lambda = 2.666 \times 10^{-6}/\theta^2$.

Table 1 compares the calculated and observed nonlinear growth rate and the decay rate for the four wavemaker amplitudes given by Barnard & Pritchard (1972), plus a larger fifth value, $\theta = 0.0120$. The agreement is generally good. For the nonlinear

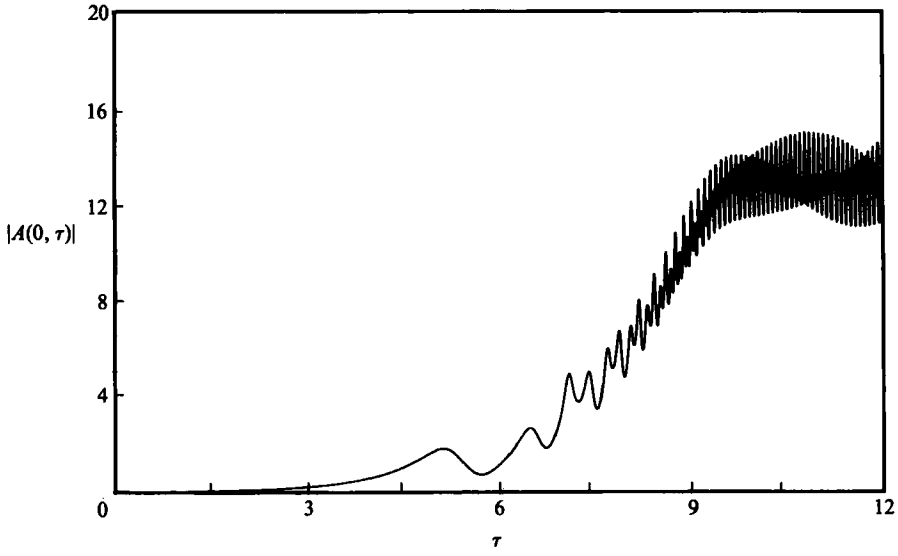

FIGURE 1. $|A(0,\tau)|$ for the inviscid case with $\lambda = 0$.

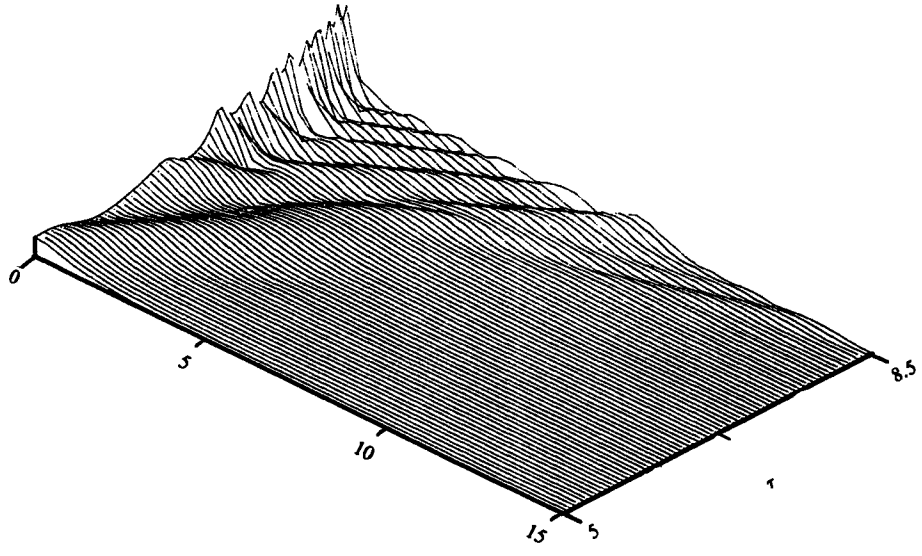

FIGURE 2. Space–time evolution of $|A(X,\tau)|$ for the inviscid case of figure 1. The vertical scale is proportional to $|A|$.

growth rate, the agreement is only fair owing to the sensitive dependence of the growth and decay rates on ω and L. At $\theta = 0.0112$, for example, a 0.1 % change in ω or a 1 % uncertainty in L results in a 5 % change in the nonlinear growth rate. The tabulated predicted decay rate is the maximum value.

Figure 3 shows $|A(0,\tau)|$ for the wavemaker amplitudes of table 1, and the corresponding phases are shown in figure 4. (The case $\theta = 0.0092$ is omitted as it is similar in appearance to $\theta = 0.0089$.) For the smaller forcing amplitudes, $A(X,\tau)$

	1	2	3	4	5
Wavemaker amplitude, θ (rad)	0.0089	0.0092	0.0099	0.0112	0.0120
Growth rate beyond the initial development (s^{-1})	0.028 (0.056)	0.033 (0.059)	0.049 (0.071)	0.073 (0.112)	0.120
Decay rate during the modulation (s^{-1})	0.027 (0.043)	0.038 (0.047)	0.072 (0.063)	0.150 (0.136)	0.274
Modulation period (s)	—	—	—	72 (69)	29

TABLE 1. Comparison of the numerical results with the experiments (in parentheses) of Barnard & Pritchard (1972)

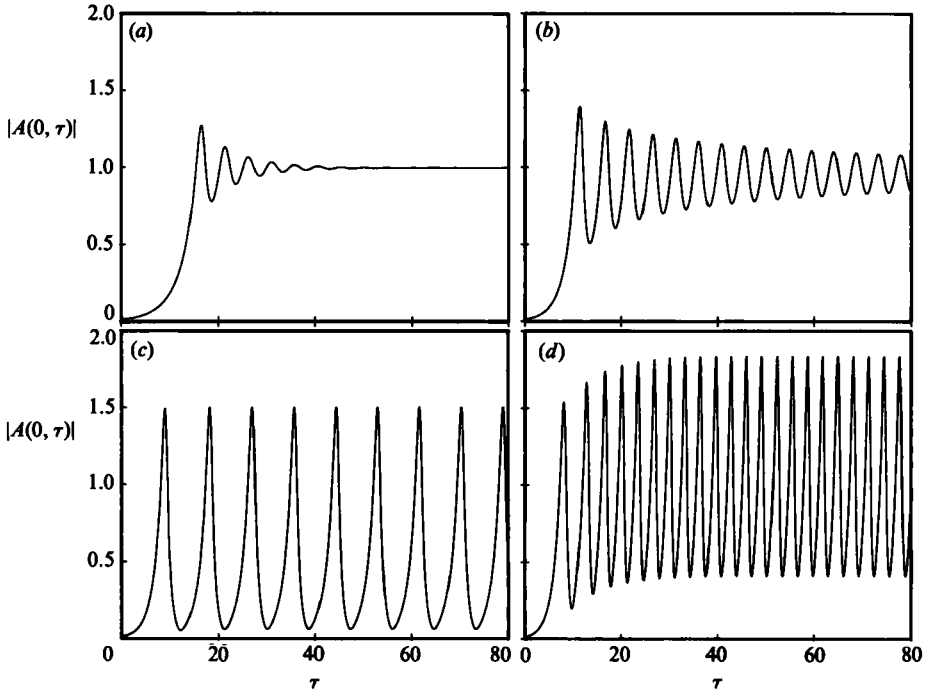

FIGURE 3. $|A(0,\tau)|$ for (*a*) $\theta = 0.0089$; (*b*) 0.0099; (*c*) 0.0112; (*d*) 0.0120.

approaches a steady state (see also figure 5*a*). For $\theta = 0.0112$ and 0.0120, the long-time behaviour of $|A(0,\tau)|$ is slowly modulated and the phase varies from $-\pi$ to π. From the phase results, it is apparent that at these higher forcing amplitudes, disturbances are propagating away from the wavemaker. In fact, 'the cross-waves never reach a true state of equilibrium, [and] after the cross-wave amplitude has passed through a maximum, a wave detaches itself from the wavemaker, propagates along the channel' and eventually decays (Barnard & Pritchard 1972, p. 254). This quotation from their experimental observations is also fitting for the numerical results, as is borne out by the space–time evolution, figure 5.

The predicted $|A(0,\tau)|$ for $\theta = 0.0112$ can be compared to Barnard & Pritchard's (1972) measurements (their figure 5) of the slow-time modulation. The observed period of the slow modulation is approximately 69 s and the maximum amplitude

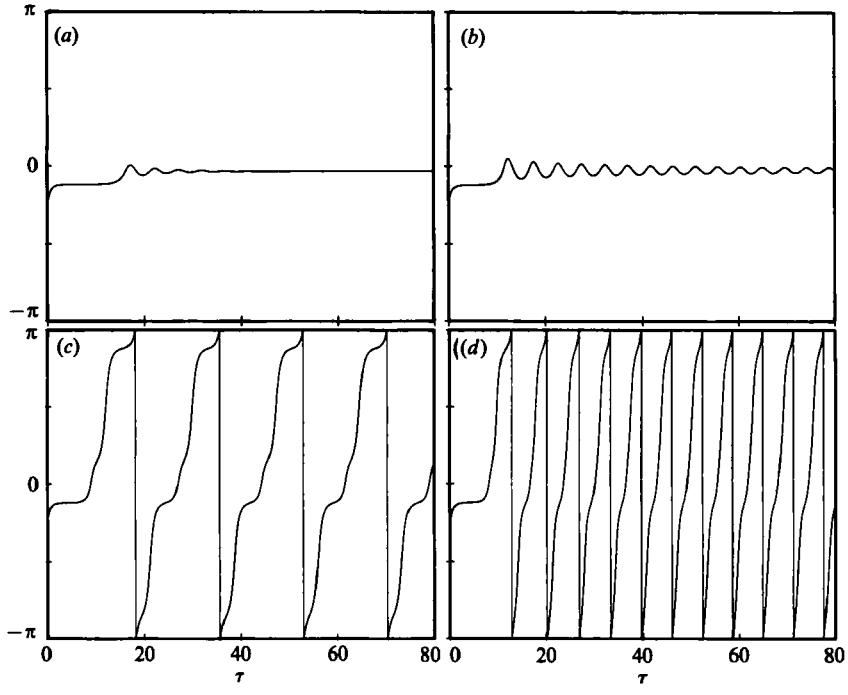

FIGURE 4. Phase of $A(0,\tau)$ for (a) $\theta = 0.0089$; (b) 0.0099; (c) 0.0112; (d) 0.0120.

is reported to be 2.75 cm.† The predicted period of 72 s is close to the measured period. The predicted maximum amplitude at the wavemaker, 1.9 cm, is comparable with the measurement.

Barnard & Pritchard (1972, p. 254) also observed that 'it is clear to the eye that the larger the value of θ, the smaller is the extent of the wave along the channel'. The numerical results, figure 6, similarly show the narrow profile of the wave at the larger forcing amplitudes; when dimensional units are restored, the effect is even more obvious.

In their study of the time-independent nonlinear Schrödinger equation describing waves forced by an antisymmetric wavemaker, Barnard *et al.* (1977) showed that the phase varied linearly along the channel in the inviscid approximation. It is interesting to note in the present study, figure 7, that, even when time dependence is present, the variation of phase along the channel is very nearly linear, especially at small wavemaker amplitudes.

There is some interest in trapped solutions for which there is no radiation away from the vicinity of the wavemaker. Trapped solutions have been found experimentally by Wu *et al.* (1984) for Faraday resonance in a vertically oscillated trough. Miles (1985) has found a trapped solution for inviscid cross-waves which is independent of the slow time τ. His condition for trapping is (in our notation) $-\lambda > 1$. However, the inviscid linear stability margin is given by $|\lambda| = 1$, and this means that the inviscid trapped solution found by Miles is, at best, neutrally stable.

Furthermore, as pointed out by Miles (1985), in the absence of the wavemaker (i.e. $R = 0$), the trapping condition implies that the wavemaker operates below the cutoff

† Though not reported in their original paper, the amplitude measurement was made at 20.8 cm from the wavemaker (W. G. Pritchard, private communication).

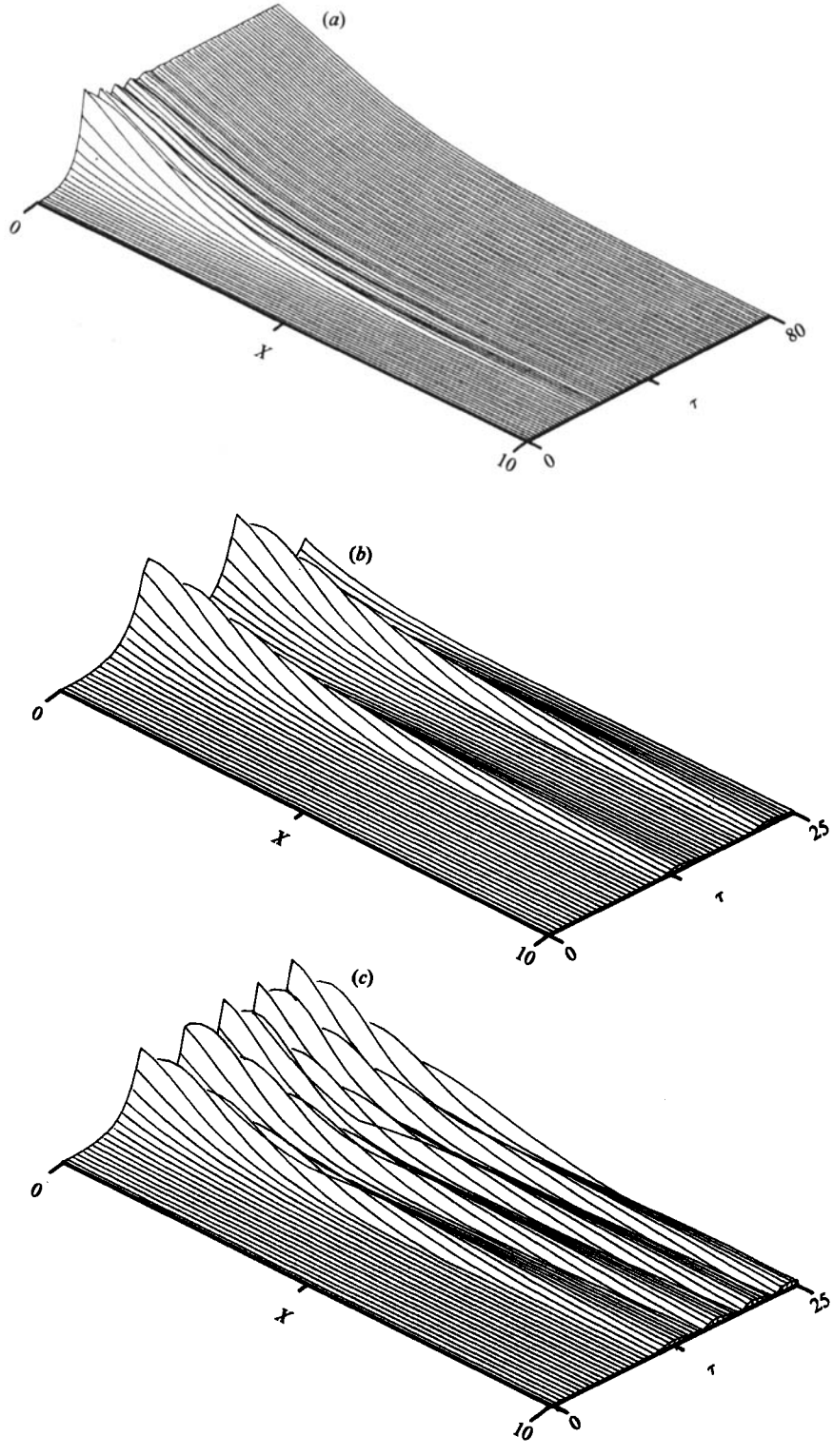

FIGURE 5. Space–time evolution for (*a*) $\theta = 0.0089$; (*b*) 0.0112; (*c*) 0.0120. The vertical scale is proportional to $|A|$.

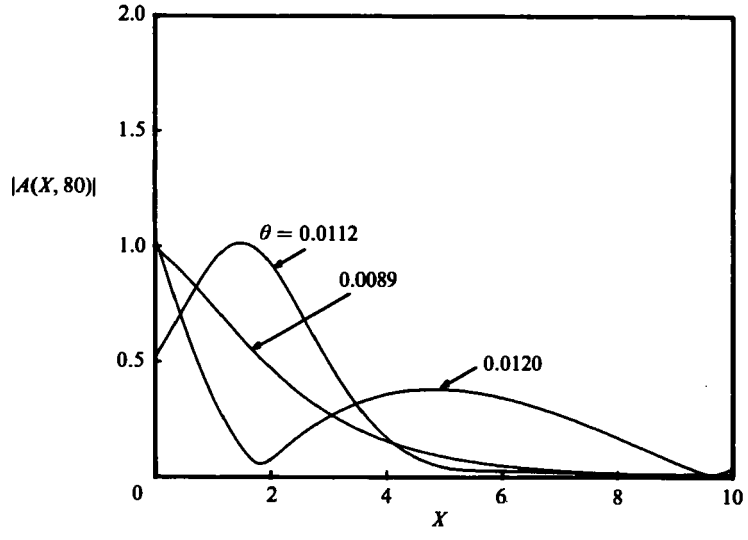

FIGURE 6. $|A(X, \tau)|$ at $\tau = 80$.

frequency. While this condition is consistent with Aranha *et al.*'s (1982) inviscid numerical results, the dissipative results give a more complicated picture. Figures 3 (a, b) and 4 (a, b) show steady trapped solutions in the long-time limit at small forcing amplitudes. Note that the phase varies along the channel, figure 7 (a), instead of being constant as indicated by the solution given by Miles. If the forcing amplitude θ is now fixed and the detuning is varied, a steady trapped solution is found for frequencies above the cutoff, $\lambda > 0$, figures 8 (a) and 9 (a). For $\lambda < 0$, figures 8 (b) and 9 (b), a time-dependent trapped solution is found for which, during each slow modulation period, the location of maximum amplitude propagates away from the wavemaker and then, rather than radiating to $X \to \infty$, returns to the wavemaker location, $X = 0$.

The occurrence of a trapped or a propagating solution has a profound effect on the appearance of the far field. Figure 10 shows the wave field ζ at $\tau = 80$. Once again, parameters are chosen to correspond to Barnard & Pritchard's (1972) wave tank. For the trapped solution at small forcing amplitudes, the crest of the non-propagating cross-wave extends from $X = 0$ well into the wave field. For larger forcing amplitudes, the disturbances which have propagated away from the wavemaker form a staggered arrangement of crests and troughs in the far field.

6. Discussion

Comparison of the linear theory with experiment for the initial linear growth and the margin of stability has been discussed in detail by Jones (1984) for the case $n = 2$. He finds very good agreement.† Our main concern is with the nonlinear results for which no previous comparison with data has appeared. In fact, Jones notes that 'there is no likelihood of the [nonlinear] results agreeing with experiment' (p. 73). He did not need to be so pessimistic as his analytic method, once rescaled and with a consideration of damping, yields equations that agree with experiments. However, this agreement is made clear only from the numerical results, and here one cannot,

† In Jones's equations (41) and (42), the '+' sign preceding the detuning term should be '−'.

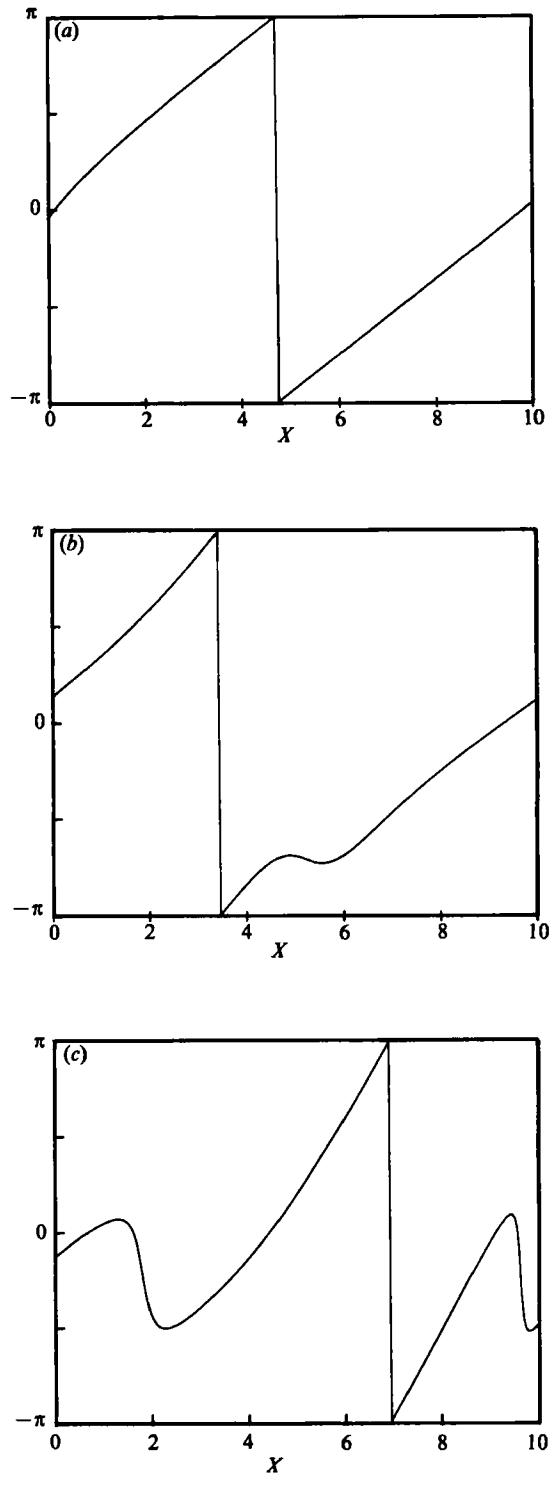

FIGURE 7. Phase of $A(X, 80)$ for (*a*) $\theta = 0.0089$; (*b*) 0.0112; (*c*) 0.0120.

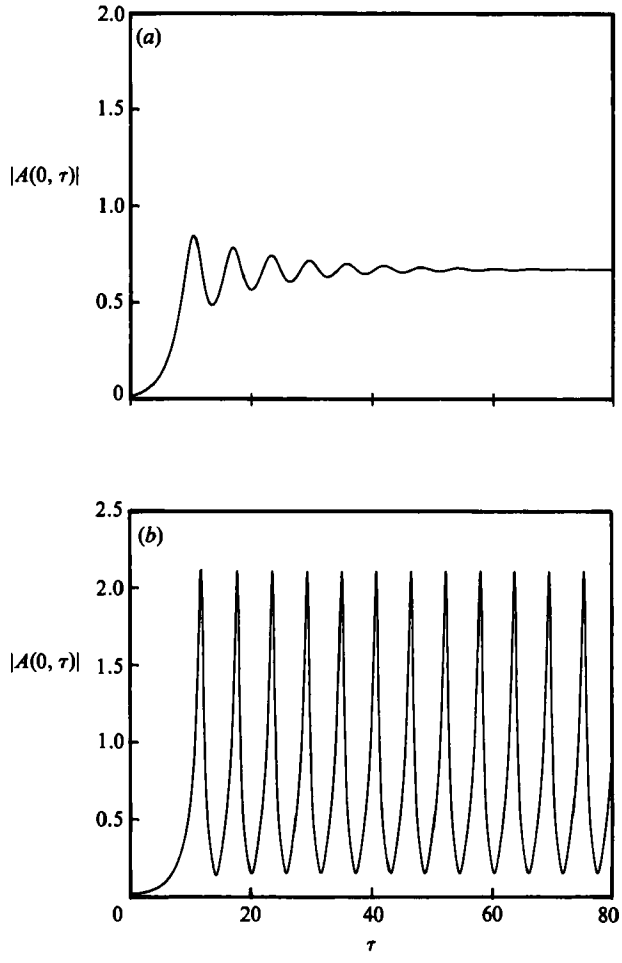

FIGURE 8. The influence of the detuning λ on $|A(0,\tau)|$ at constant forcing amplitude, $\theta = 0.0112$, for (*a*) $\lambda = 0.5$; (*b*) -0.5.

as in Jones, limit the results to the case $A = 0$. More seriously, the computations are rather sensitive to the end condition, and the choice of $X = 1$ as the downstream limit in Jones's inviscid model is prone to yield spurious results.

In summary, the present work favourably describes the experimental results for linear and nonlinear growth rates, slow modulation period, cross-wave amplitude, and trapped and propagating behaviour. The exponential growth predicted by the linearized equation is curtailed by nonlinearity with no necessity for dissipation. The numerical results indicate that the conditions for which trapped solutions occur are quite different from those indicated by the inviscid analysis. Also, at higher forcing amplitudes, it is found that cross-waves propagate away from the wavemaker to form a staggered arrangement of crests in the far field. It is interesting to note that the variation of crest arrangement to the staggered pattern which occurs by increasing the wavemaker amplitude was often observed in our wave tank, which has a geometry similar to the one used by Barnard & Pritchard (1972) but operates at a higher angular frequency, $\Omega \approx 31\ \mathrm{s}^{-1}$.

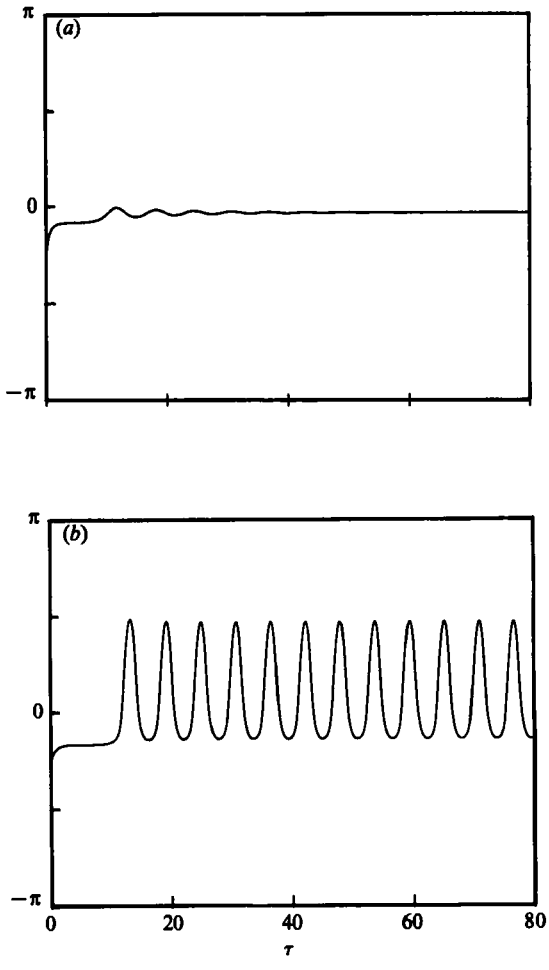

FIGURE 9. The influence of the detuning λ on the phase of $A(0,\tau)$ at constant forcing amplitude, $\theta = 0.0112$, for (*a*) $\lambda = 0.5$; (*b*) -0.5.

Comparison with experiment reveals, as well, the limitations of the perturbation equations. The model relies on an empirical damping coefficient which is found to depend on wave amplitude. Analytical expressions (as opposed to the empirical fit) for linear dissipation (Barnard *et al.* 1977; Miles 1984) also need further refinement as they yield damping coefficients that are, in general, too small. We are presently investigating dissipative effects, including the effect of dissipation at the wavemaker. Additionally, at large forcing amplitudes, the cross-wave profile in the X-direction is observed to be more variegated than the numerical model allows. Experiments at wavelengths of approximately 5 cm reveal profiles that are more step-like than smoothly decaying in the X-direction. Finally, at extremely large forcing amplitudes, the weakly nonlinear assumption may not be suitable.

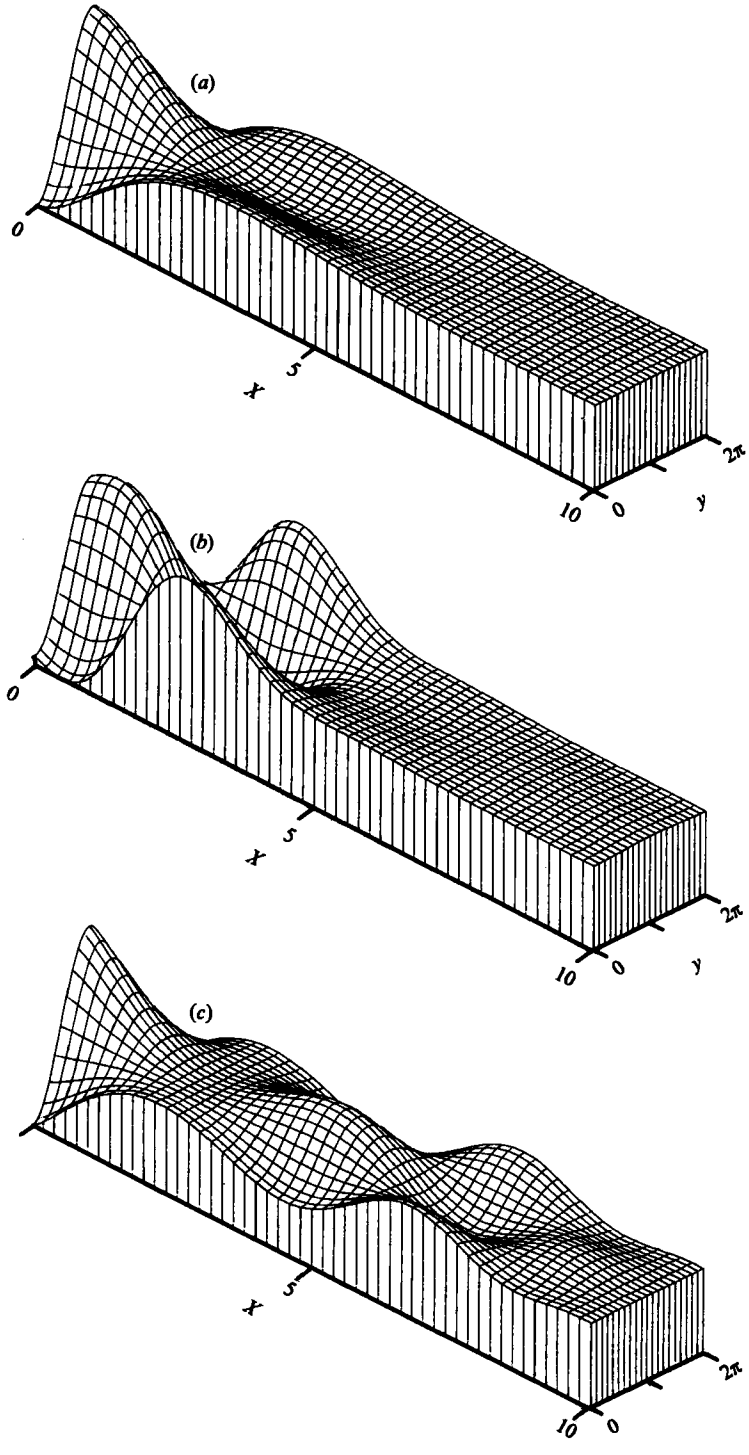

FIGURE 10. A numerical snapshot of the wave field at $\tau = 80$ for (*a*) $\theta = 0.0089$; (*b*) 0.0112; (*c*) 0.0120. The vertical scale is proportional to ζ.

National Science Foundation support through a Research Initiation Award (MEA-8404821) is gratefully acknowledged. S. Lichter would like to thank A. Bernoff for several discussions during the IUTAM Symposium on Fluid Mechanics in the Spirit of G. I. Taylor. The authors are grateful for receipt of a preprint of related work by J. W. Miles and J. Becker. We also thank the referees for their generous insights into the scaling.

REFERENCES

ARANHA, J. A., YUE, D. K. P. & MEI, C. C. 1982 Nonlinear waves near a cut-off frequency in an acoustic duct – a numerical study. *J. Fluid Mech.* **121**, 465–485.

BARNARD, B. J. S., MAHONY, J. J. & PRITCHARD, W. G. 1977 The excitation of surface waves near a cut-off frequency. *Phil. Trans. R. Soc. Lond.* A **286**, 87–123.

BARNARD, B. J. S. & PRITCHARD, W. G. 1972 Cross-waves. Part 2. Experiments. *J. Fluid Mech.* **55**, 245–255.

CILIBERTO, S. & GOLLUB, J. P. 1985 Chaotic mode competition in parametrically forced surface waves. *J. Fluid Mech.* **158**, 381–398.

GARRETT, C. J. R. 1970 On cross-waves. *J. Fluid Mech.* **41**, 837–849.

HAVELOCK, T. H. 1929 Forced surface waves on water. *Phil. Mag.* **8**, 569–576.

JONES, A. F. 1984 The generation of cross-waves in a long deep channel by parametric resonance. *J. Fluid Mech.* **138**, 53–74.

LICHTER, S. & SHEMER, L. 1986 Experiments on nonlinear cross waves. *Phys. Fluids* **29**, 3971–3975.

MAHONY, J. J. 1972 Cross-waves. Part 1. Theory. *J. Fluid Mech.* **55**, 229–244.

MILES, J. W. 1984 Parametrically excited solitary waves. *J. Fluid Mech.* **148**, 451–460.

MILES, J. W. 1985 Note on a parametrically excited, trapped cross-wave. *J. Fluid Mech.* **151**, 391–394.

WU, J., KEOLIAN, R. & RUDNICK, I. 1984 Observation of a nonpropagating hydrodynamic soliton. *Phys. Rev. Lett.* **52**, 1421–1424.